

Appendix 3

Island perturbation to the sky radiance over the ocean: Simulations

by

Haoyu Yang, Howard R. Gordon, and Tianming Zhang

The authors are with the Department of Physics, University of Miami, Coral Gables, FL 33124.

(Submitted to *Applied Optics*)

**Acknowledgement**

We are grateful to the National Aeronautics and Space Administration for support under Grant NAGW-273 and Contracts NAS5-31363 and NAS5-31743, and the Office of Naval Research under Grant Number N00014-89-J-1985.

## Abstract

We demonstrate, through Monte Carlo simulations, that significant perturbations to sky radiance measurements over the ocean can occur when measurements are carried out using radiometers located on islands. In particular, we present examples of the influence of the physical and optical thicknesses of an aerosol layer, the azimuth of observation relative to the sun, the size of the island, the location of the radiometer on the island, and the albedo of the island, on the magnitude of the perturbation for a circular island of uniform albedo. Relative errors in sky radiance of as high as 39% were found in the blue. Simulated (perturbed) sky radiances were combined with an algorithm for retrieving the aerosol phase function  $P(\Theta)$ , where  $\Theta$  is the scattering angle, and single scattering albedo  $\omega_0$ , to demonstrate how the perturbation can influence their retrieved values. It was found that the fractional error in the retrieved values of the product  $\omega_0 P(\Theta)$  can be significantly greater than that in the sky radiance, because of the effects of multiple scattering. This underscores the importance of removing the island perturbation prior to employing an inversion algorithm. Fortunately, the relative sky radiance perturbation is a weak function of  $P(\Theta)$ , so a correction is feasible.

## 1. Introduction

There is a need to understand the columnar properties of aerosols over the ocean (a) for atmospheric correction<sup>1</sup> of ocean color sensors, e.g., the Sea-viewing wide-field-of-view sensor (SeaWiFS),<sup>2</sup> and (b) for aiding retrieval of aerosol properties over the ocean from similar instruments.<sup>1,3</sup> Wang and Gordon<sup>4</sup> have presented a method for retrieving the aerosol columnar phase function and single scattering albedo from measurements of the aerosol optical thickness and sky radiance over the ocean, through iteratively solving the radiative transfer equation (RTE) until the measured and predicted (based on the aerosol phase function and single scattering albedo) sky radiance agree within experimental error. Their method was an extension of earlier work by King,<sup>5</sup> Box and Deepak,<sup>6,7</sup> Nakajima et al.,<sup>8</sup> and Wendisch and von Hoyneunegn-Huene,<sup>9</sup> and basically works because the surface albedo of the ocean is low and known. The ideal platform for such measurements is a ship; however, for a variety of reasons, e.g., cost and the simplicity of a stable platform, it is more convenient to locate instruments on islands. Unfortunately, even a small island will perturb the light field in its vicinity if its albedo is significantly different from that of the ocean. It is important to have an understanding of the extent of such perturbations to determine the suitability of potential station locations and, perhaps, to provide a first-order correction for the effect. In this paper we present the results of simulations aimed at providing an assessment of the possible extent of the perturbation.

We begin by describing the Monte Carlo simulation techniques we developed for this problem in the special case that the island is a circular disk. Then we operate the simulation code to provide examples of the sky radiance perturbation as a function of the size of the island, the optical thickness of the aerosol, the physical thickness of the aerosol layer, the position of the sensor on the island, and the albedo of the island. Finally, we apply the aerosol retrieval technique of Wang and Gordon<sup>4</sup> to simulated measurements and show how the island perturbation influences the retrieval of the phase function. In an appendix we provide an alternate Monte Carlo approach that is applicable to an island of any shape. A code based on this approach could be used to provide a first-order correction to the perturbation.

## 2. Computational Procedure

The distribution and propagation of light field in the atmosphere is governed by the radiative transfer equation (RTE). There are several ways to solve the equation for a plane parallel atmosphere where the light field is invariant to translation in all directions parallel to the boundaries. However, in the presence of a perturbation that destroys this invariance (the island), the Backward Monte Carlo (BMC) method is the most straightforward. In the BMC procedure, the photon paths are simulated from the detector to the source. The procedure begins with the emission of a photon from the detector in a direction exactly opposite to the direction in which the radiance is desired. The distance the photon travels before interacting in the medium is determined from random sampling based on the beam attenuation coefficient of the medium. Upon scattering, the new direction the photon travels is generated by sampling the scattering phase function. When the photon is scattered, however, it may strike the surface of the sea or the surface of the island. In the former case the direction of the photon is determined from Fresnel's laws of reflection, while in the latter case the new direction is sampled from the bidirectional reflection distribution function (BRDF) of the island. At each interaction with the medium, the possibility that the photon will be scattered in a direction which would allow it to propagate to the sun, either directly, or by reflection from the sea surface or the island, is computed and collected.

Figure 1 describes the geometry of the RTE problem. The atmosphere is assumed to be composed of two layers, with aerosol scattering confined to the lower layer and molecular scattering to the upper layer. The lower boundary of the medium is the ocean. The island is assumed to be circular in shape (radius  $R$ ) and to be a lambertian reflector. The radiometer is placed anywhere on the island. The  $z$ -axis is normal to the sea surface and is directed upward from the center of the island. The  $x$ -axis is the projection of the solar beam on the sea surface. The  $y$ -axis is determined by the right-hand-rule.

There are three paths the photon can take toward the sun at each interaction in the atmosphere: (1) the photon can be scattered in a direction toward the sun; (2) it can be scattered toward the sea surface and Fresnel-reflected toward the sun; or (3) it can be scattered toward the island and be diffusely reflected by the island in a direction toward the sun. In each case the Monte Carlo

estimator is related to the probability that the photon will exit the atmosphere toward the sun. At the  $n^{\text{th}}$  interaction for a given photon, the contribution to the radiance from the first path,  $L_1$  is simply

$$L_1 = \omega_0^n P(\Theta_1) \bar{T}(\text{interaction} \rightarrow \text{sun}) \quad (1)$$

where  $\omega_0$  and  $P(\Theta)$  are the single scattering albedo and scattering phase function of the atmosphere (for a scattering angle  $\Theta$ ) at the interaction point,  $\Theta_1$  is the angle between the direction of propagation of the photon from the previous interaction point and a vector from the present interaction point to the sun, and  $T(\text{interaction} \rightarrow \text{sun})$  is the atmospheric transmittance of the atmosphere from the interaction point to the top of the atmosphere in the direction of the sun. Likewise, the contribution to the radiance from path 2,  $L_2$ , is

$$L_2 = \omega_0^n P(\Theta_2) T(\text{interaction} \rightarrow \text{surface} \rightarrow \text{sun}) R_f, \quad (2)$$

where  $\Theta_2$  is the angle between the direction of propagation of the photon from the previous interaction point and a vector from the present interaction to the sea surface in such a direction that, if followed by a photon, it would be Fresnel-reflected in a direction toward the sun.  $T(\text{interaction} \rightarrow \text{surface} \rightarrow \text{sun})$  is the transmittance of the atmosphere from the present interaction point to the sea surface and then from the sea surface to the top of the atmosphere in a direction toward the sun.  $R_f$  is the Fresnel reflectivity of the air-sea interface.  $R_f$  is set to zero if the path — interaction → surface — intersects the island, i.e.,  $L_2 = 0$  if the island prevents specular reflection from the surface in the direction of the sun.

The contribution from the third process — scattering toward the island followed by diffuse reflection from the island toward the sun — is more complex. This is because at each interaction the contribution,  $L_3$ , to the radiance is an integral over all possible paths that the photon can take toward the island and then be scattered by the island toward the sun. It is given by

$$L_3 = \omega_0^n \int P(\hat{\xi}'' \rightarrow \hat{\xi}') P_I(\hat{\xi}' \rightarrow \hat{\xi}_0) T(\hat{\xi}') T(\hat{\xi}_0) d\Omega(\hat{\xi}'),$$

where  $\hat{\xi}''$  is a unit vector from collision  $n - 1$  to collision  $n$ ,  $\hat{\xi}'$  is a unit vector from collision  $n$  to a point on the island (Figure 1), and  $\hat{\xi}_0$  is a unit vector from a point on the island in a direction

toward the sun,  $T(\hat{\xi}')$  is the atmospheric transmittance from collision  $n$  to the island in the direction  $\hat{\xi}'$ , and  $T(\hat{\xi}_0)$  is the atmospheric transmittance from the island to the sun.  $d\Omega(\hat{\xi}')$  is a differential in solid angle around the direction  $\hat{\xi}'$ , and  $P_I(\hat{\xi}' \rightarrow \hat{\xi}_0)$  is the probability that radiance propagating in the direction  $\hat{\xi}'$  will be scattered by the island in the direction  $\hat{\xi}_0$ . Since the island is lambertian,

$$P_I(\hat{\xi}' \rightarrow \hat{\xi}_0) = \frac{A}{2\pi} \cos \theta_0,$$

where  $A$  is the albedo of the island and  $\theta_0$  is the solar zenith angle. Thus,

$$L_3 = \frac{A}{2\pi} \cos \theta_0 T(\hat{\xi}_0) \omega_0^n \int P(\hat{\xi}'' \rightarrow \hat{\xi}') T(\hat{\xi}') d\Omega(\hat{\xi}'). \quad (3)$$

Note that this is actually a double integral and that it must be evaluated at each collision. Thus, the key to including the island effects in the radiative transfer process is the evaluation of Eq. (3) at each collision. A simple possibility for evaluating the integral is to replace it by a Monte Carlo estimate, i.e., if  $\hat{\xi}'$  is chosen from a uniform distribution of directions within  $\Omega'$ , the solid angle subtended by the island at the collision point, then

$$\lim_{N \rightarrow \infty} \frac{1}{N} \sum_{i=1}^N P(\hat{\xi}'' \rightarrow \hat{\xi}'_i) T(\hat{\xi}'_i) = \int P(\hat{\xi}'' \rightarrow \hat{\xi}') T(\hat{\xi}') d\Omega(\hat{\xi}'), \quad (4)$$

where the index  $i$  refers to one of the  $N$  individual samples of  $\hat{\xi}'$ . However, we still need to compute the solid angle  $\Omega'$  (Figure 1) in order to normalize the uniform probability density used to compute  $\hat{\xi}'$ . This is also a double integral. Fortunately, it can be determined directly as a sum of elliptic integrals when the island is circular in shape; however, in the general case the evaluation of  $\Omega'$  cannot be carried out analytically.

It is possible to avoid evaluation of  $\Omega'$  by replacing  $d\Omega(\hat{\xi}')$  by  $|\hat{\xi}' \bullet \hat{n}'| dA(\hat{\xi}')/r'^2$ , where  $dA$  is the island area subtended by the solid angle  $d\Omega(\hat{\xi}')$ ,  $r'$  is the distance from the interaction point to  $dA$ , i.e.,  $\sqrt{(x - x')^2 + (y - y')^2 + z^2}$ , and  $\hat{n}'$  is the unit normal to the island surface at the position of  $dA$ . Now, the point  $(x', y', 0)$  on the island is chosen from a uniform distribution in area, and the estimator becomes

$$\lim_{N \rightarrow \infty} \frac{1}{N} \sum_{i=1}^N \frac{|\hat{\xi}' \bullet \hat{n}'|}{r'^2} P(\hat{\xi}'' \rightarrow \hat{\xi}'_i) T(\hat{\xi}'_i) = \int P(\hat{\xi}'' \rightarrow \hat{\xi}') T(\hat{\xi}') d\Omega(\hat{\xi}'). \quad (5)$$

Thus, the price of avoiding the computation of  $\Omega'$  is the introduction of a singularity in this portion of the estimator for  $L_3$ . Clearly, photons that interact with the atmosphere close to the island will make a large contribution to  $L_3$ , which will increase the variance of the estimate. The obvious method of coping with the singularity is to use Eq. (4) for photons close to the island, and Eq. (5) elsewhere. In our Monte Carlo code, satisfactory results are obtained if Eq. (5) is used whenever the interaction point  $(x, y, z)$  is at a distance greater than  $0.1R$  from any point on the island. Evaluation of the integrals in Eqs. (4) or (5) requires splitting the photon into  $N$  components (each with weight  $1/N$ ) at each interaction; however, we found that such splitting did not improve the accuracy of the results appreciably, so the integral in question was evaluated at each interaction with  $N = 1$ .

### 3. Atmospheric Models

In our simulations we assume that the atmosphere consists of two homogeneous layers with the aerosols in the lower layer, and the molecular scattering (Rayleigh scattering) in the upper layer. The physical thickness of the lower layer,  $h$  is taken to be 1 or 2 km. The optical characteristics of the aerosol were generated from the models provided by Shettle and Fenn.<sup>10</sup> In particular, we used the model size distributions and refractive indices for their Tropospheric model at a relative humidity (RH) of 80% (which we indicate by T80) and the Gordon and Wang<sup>1</sup> Coastal model, which is based on a combination of Shettle and Fenn's Tropospheric and Oceanic models with RH = 80% (designated as C80) to generate the scattering phase functions corresponding to a wavelength of 443 nm. These are provided in Figure 2. For all of our computations the single scattering albedo of the aerosol was taken to be unity.

### 4. Assessment of the impact of the island on sky radiance

In this section we present the results of simulations in which we vary the values of the significant parameters:  $R$  — the radius of the island;  $h$  — the physical thickness of the aerosol;  $\tau_a$  — the aerosol optical thickness;  $\phi$  — the azimuth of the viewing direction relative to the sun (solar azimuth is at  $\phi = 0$ ); the position of the sensor on the island; and the aerosol phase function. Unless otherwise

stated, the Rayleigh optical thickness,  $\tau_r$ , is taken to be 0.25 (wavelength  $\sim 437$  nm), C80 is used as the aerosol model to generate the aerosol phase function, and the albedo ( $A$ ) of the island is unity.

Since our computations carried out using the Monte Carlo methods and have an inherent statistical error, it is important to understand the accuracy with which they are performed. To effect this, we have carried out one simulation in which  $10^7$  photons were ejected from the source at  $\phi = 90^\circ$  with  $\tau_r = \tau_a = 0.25$  and  $h = 2$  km. Both the solar zenith angle,  $\theta_0$ , and the viewing angle,  $\theta_v$ , were  $60^\circ$ , i.e., viewing was in the almucantar of the sun. The resulting  $L_t = L_1 + L_2 + L_3$  was tabulated for each  $10^4$  photons. The average of  $L_t$ , normalized to the extraterrestrial solar irradiance ( $F_0$ ), was 0.052075 for the  $10^7$  photons. In this manner, we have  $10^3$  independent simulations. For each of the  $10^3$  independent simulations the number of occurrences of  $L_t$  were binned in increments of 0.0005, e.g., the number of occurrences of  $L_t$  in ranges 0.0500 to 0.0505, 0.0505 to 0.0510, etc. were recorded. Figure 3 provides the resulting histogram of the number of occurrences. For this case, it is seen that the standard deviation of the distribution is  $\sim 0.0016$ , or the statistical error in  $L_t$  when  $10^4$  photons are released from the detector is  $\sim 3\%$ . In most of our simulations, between  $10^6$  and  $10^7$  photons are processed, so the relative error in this case would be  $\sim 0.3$  to  $0.1\%$ . In the light of Figure 3, the statistical error in the magnitude of  $L_t$  is expected to be well below the perturbation in the magnitude of  $L_t$  caused by the presence of the island (see Figure 4b in particular where the perturbation in  $L_t$  was  $\sim 25\%$  for this case). Had we employed Eq. (5) at all of the interactions, rather than using Eq. (4) when the interaction was close to the island, the principal difference between the resulting histogram and Figure 3 is the occasional occurrence of a large value of  $L_t$ , e.g.,  $L_t \approx 0.094$  was obtained once in 1000 simulations. In the absence of the island, our BMC code reproduces the radiances computed with a successive order of scattering code<sup>11,12</sup> within 0.1–0.2%. Also,  $L_t$  approaches that for a plane parallel atmosphere bounded by a lambertian surface of infinite extent as  $R$  becomes large.

The influence of the variation of  $\tau_a$  and  $h$  on the radiance  $L$ , normalized to  $F_0$ , in the almucantar of the sun ( $\theta_v = \theta_0$ ) with  $\theta_0 = 60^\circ$ , is presented in Figures 4a, 4b, and 4c corresponding to  $\phi = 0$ ,  $90$ , and  $180^\circ$ , respectively. In this figure the sensor is located at the center of the island, and

symmetry dictates that the additional radiance caused by the presence of the island ( $L_3$ ) is the same for all viewing directions (this is satisfied in our computations); however, the contribution from specular reflection by the sea surface ( $L_2$ ) will depend on the viewing angle by virtue of the island's blocking of a portion of the sea surface. Thus, the perturbation caused by the island will have a weak dependence on the viewing azimuth. The computations clearly demonstrate the effect of an increasing radiance measured as the size of the island is increased. As expected, the perturbation is most significant in viewing directions for which the radiance in the absence of the island is small, i.e., directions far from the solar aureole. The perturbation is seen to increase very slowly with  $\tau_a$ , e.g., for  $h = 2$  km and  $\phi = 90^\circ$ , the relative error in the sky radiance,  $\Delta L_t/L_t$ , only increases from 18% to 29% as  $\tau_a$  increases from 0.1 to 0.5. Decreasing the thickness of the aerosol layer, but keeping  $\tau_a$  fixed, is seen to increase the perturbation, as this increases the probability that an aerosol-scattered photon will interact with the island. Thus, we see that even for a relatively small island, e.g.,  $R \sim 1$  km, the perturbation of the radiance can reach nearly 10% in some of the examples provided here.

One obvious method of reducing the perturbation is to move the sensor to the edge of the island such that  $\phi = 0$  corresponds to the sensor viewing the sun in line with the center of the island. In this manner, measurements at  $\phi \geq 90^\circ$  would be carried out looking over open water. Note that in this case the symmetry is broken and the radiance added by the presence of the island ( $L_3$ ) is no longer independent of  $\phi$ . Figures 5a, 5b, and 5c compare the resulting perturbations computed for  $h = 1$  km when this strategy is employed. For  $\phi = 180^\circ$  (Figure 5c), there is a significant decrease (as much as 90%) in the island perturbation, while for  $\phi = 90^\circ$  (Figure 5b) the decrease is considerably less, i.e.,  $\sim 50 - 70\%$ . For  $\phi = 10^\circ$  (Figure 5a) there is essentially no change in the perturbation, and this implies there is a net gain in the accuracy of the measured sky radiance by moving the sensor from the center to the edge of the island.

Figure 6 provides an example of the change in the perturbation when the island albedo is reduced from 1.0 to 0.5. In the example shown, for  $R \lesssim 2$  km the perturbation is reduced by  $\sim 1/2$ , suggesting that for small islands photons usually interact once with the island. In contrast,

for  $R = 8$  km the perturbation is reduced to  $\sim 40\%$  of its original value indicating multiple interactions with the island.

In Figure 7 we provide an example of the influence of the shape of the aerosol phase function on the perturbation of the light field. The figure compares the magnitude of the perturbations when the aerosol phase functions are computed using the C80 and T80 aerosol models (Figure 2), and shows that  $\Delta L_t/L_t$  is a weak function of the aerosol phase function. This suggests that a correction for the island perturbation may be possible with only a coarse estimate of the aerosol phase function.

## 5. Impact on retrieval of aerosol optical properties

In this section, we provide examples of the influence of the island perturbation on the retrieval of aerosol optical properties. For this, we apply the method described by Wang and Gordon<sup>4</sup> for retrieving the columnar aerosol phase function and single scattering albedo from measurements of  $\tau_a$  and the sky radiance  $L_t$  in the solar almucantar and the principal plane. Pseudodata was generated for an island with  $R = 5$  km,  $A = 1$ , and  $\theta_0 = 60^\circ$ , with the sensor located at the center and at the edge of the island. The aerosol optical properties were taken from the C80 aerosol model (with  $\omega_0 = 1$ ), and the physical and optical thicknesses of the aerosol layer were, respectively, 1 km and 0.25. Figure 8 provides the fractional error in  $L_t$  in the solar almucantar induced by the island for both sensor positions. Note the significant improvement obtained for  $\phi \gtrsim 90^\circ$  by moving the sensor from the center to the edge of the island. Figure 9 shows the excellent retrieval of the phase function for  $\Theta \lesssim 145^\circ$  in the absence of the island. Note that for  $\Theta \gtrsim 145^\circ$  the values of  $\omega_0 P$  are (exponentially) extrapolated to  $180^\circ$  using the last five points for  $\Theta > 120^\circ$ . This extrapolation is used to complete the phase function for the iterative retrieval procedure and for estimating the value of  $\omega_0$ . In this simulation, the retrieved value of  $\omega_0$  was 0.984 compared to the correct value of unity. In Figure 10 we show retrievals obtained with the sensor on the island. The strong perturbation by the island manifests in values of  $\omega_0 P(\Theta)$  that are too large. In fact, the fractional error in  $\omega_0 P(\Theta)$  can be as much as a factor of two for some values of  $\Theta$  when the sensor is at the center of the island. This causes the retrieved values of  $\omega_0$  to even be  $> 1$  (1.04 and 1.12

using the island edge and center pseudodata, respectively). Note that the placing of the sensor at the edge does not completely solve the perturbation problem. There is still significant error for  $40^\circ \lesssim \Theta \lesssim 80^\circ$ . It should be possible to remove much of this error by using the retrieved phase function to correct  $L_t$  for the island's perturbation.

## 6. Concluding remarks

In this paper we have demonstrated through simulations that significant perturbations to the sky radiance over the ocean can occur when measurements of  $L_t$  are carried out using radiometers located on islands. In particular we showed how the physical and optical thicknesses of the aerosol, the azimuth of observation relative to the sun, the size of the island, the location of the radiometer on the island, and the albedo of the island, influence the magnitude of the perturbation, which can reach as much as  $\sim 40\%$  or more of the unperturbed radiance. We then combined the simulated (perturbed) sky radiance with an algorithm for retrieving the aerosol phase function and single scattering albedo to demonstrate how the perturbation can influence the retrieved values of  $\omega_0 P(\Theta)$ . It is interesting to note that the fractional error in the retrieved  $\omega_0 P(\Theta)$  can be significantly greater than that in  $L_t$  (compare Figure for  $\phi \gtrsim 90^\circ$  and Figure 20 for  $\Theta \gtrsim 60^\circ$ ). This effect is due to multiple scattering, and underscores the importance of the removal of the island's perturbation prior to employing an inversion algorithm. Fortunately, the perturbation  $\Delta L_t/L_t$  is a weak function of the aerosol phase function, so a correction (perhaps even an iterative procedure with the inversion algorithm) is feasible. In the following appendix we provide a modified Monte Carlo computational procedure with which one can assess the influence of an island of arbitrary shape and position-dependent albedo on  $L_t$ . Such a code could be used to effect a correction for the island perturbation.

### Appendix: An alternate computational procedure for an Island of arbitrary shape

One difficulty with our Monte Carlo approach described in Section 2 is the necessity of computing  $\Omega'$  (Figure 1) when the photon is close to the island. This computation is tractable only when the island has a simple shape, e.g., a circular disk. An alternate procedure is required for an

island of arbitrary shape. Here, we present a simple modification of the procedure presented in the text.

As described in Section 2, there are three contributions to the Monte Carlo estimator ( $L_1$ ,  $L_2$ , and  $L_3$ ). In the revised approach, the procedures for  $L_1$  and  $L_2$  are unchanged, but  $L_3$  is computed using a completely different approach. Rather than estimating the  $L_3$  contribution at each interaction (Section 2), the estimate is made only when the photon actually strikes the island. When this occurs, the estimate of  $L_3$  (assuming as before that the island is a lambertian reflector) is

$$L_3 = \frac{\omega_0^n A \cos \theta_0}{2\pi} T(\hat{\xi}_0),$$

where  $n$  is the number of collisions made by the photon before striking the island. This completely avoids the computation of  $\Omega'$ . At each interaction one need only compute  $L_1$  and then determine if the photon could specularly reflect from the surface toward the sun (to determine if  $L_2$  makes a contribution). Finally, between any two collisions one must determine if the island intersects the path, in which case  $L_3$  is given by the above equation. Clearly, an arbitrarily shaped island represents little additional difficulty. Also, a spatially dependent island albedo is straightforward to implement.

We have implemented this procedure for a circular island. Figure 11 provides the resulting statistics for the same simulation as presented in Figure 3, which used the procedure described in Section 2. Comparison of the two figures shows that the alternate technique for dealing with the island's contribution to  $L_t$  is as effective as our earlier, and more complex, approach.

## References

- [1] H. R. Gordon and M. Wang, "Retrieval of water-leaving radiance and aerosol optical thickness over the oceans with SeaWiFS: A preliminary algorithm," *Applied Optics* **33**, 443–452 (1994).
- [2] S. B. Hooker, W. E. Esaias, G. C. Feldman, W. W. Gregg and C. R. McClain, *SeaWiFS Technical Report Series: Volume 1, An Overview of SeaWiFS and Ocean Color* (NASA, Greenbelt, MD, Technical Memorandum 104566, July 1992).
- [3] M. Wang and H. R. Gordon, "Estimating aerosol optical properties over the oceans with MISR: Some preliminary studies," *Applied Optics* **33**, 4042–4057 (1994).
- [4] M. Wang and H. R. Gordon, "Retrieval of the Columnar Aerosol Phase Function and Single Scattering Albedo from Sky Radiance over the Ocean: Simulations," *Applied Optics* **32**, 4598–4609 (1993).
- [5] M. D. King and B. M. Herman, "Determination of the Ground Albedo and the Index of Absorption of Atmospheric Particulates by Remote Sensing. Part I: Theory," *Jour. Atmos. Sci.* **36**, 163–173 (1979).
- [6] M. A. Box and A. Deepak, "Retrieval of Aerosol Size Distributions by Inversion of Simulated Aureole Data in the Presence of Multiple Scattering," *Applied Optics* **18**, 1376–1382 (1979).
- [7] M. A. Box and A. Deepak, "An Approximation to Multiple Scattering in the Earth's Atmosphere: Almuquantar Radiance Formulation," *Jour. Atmos. Sci.* **38**, 1037–1048 (1981).
- [8] T. Nakajima, M. Tanaka and T. Yamauchi, "Retrieval of the Optical Properties of Aerosols from Aureole and Extinction Data," *Applied Optics* **22**, 2951–2959 (1983).

- [9] M. Wendisch and W. von Hoyningen-Huene, "High Speed Version of the Method of 'Successive Order of Scattering' and its Application to Remote Sensing," *Beitr. Phys. Atmosph.* **64**, 83–91 (1991).
  
- [10] E. P. Shettle and R. W. Fenn, *Models for the Aerosols of the Lower Atmosphere and the Effects of Humidity Variations on Their Optical Properties* (Air Force Geophysics Laboratory, Hanscomb AFB, MA 01731, AFGL-TR-79-0214, 1979).
  
- [11] H. R. Gordon and M. Wang, "Surface Roughness Considerations for Atmospheric Correction of Ocean Color Sensors. 1: The Rayleigh Scattering Component," *Applied Optics* **31**, 4247–4260 (1992).
  
- [12] H. R. Gordon and M. Wang, "Surface Roughness Considerations for Atmospheric Correction of Ocean Color Sensors. 2: Error in the Retrieved Water-leaving Radiance," *Applied Optics* **31**, 4261–4267 (1992).

## Figure Captions

Figure 1. Schematic for computing the island's contribution to the sky radiance.

Figure 2. Aerosol scattering phase functions used in the simulations.

Figure 3. Histogram of the number of occurrences of given values of  $L_t$  in intervals of  $0.0005 \times 10^{-2}$  for 1000 simulations of  $10^4$  photons each. The dotted line represents the estimate of the mean value of  $L_t$  for the  $10^7$  photons.

Figure 4. Computed value of  $L_t$  as a function of  $R$  for C80,  $\theta_v = \theta_0 = 60^\circ$ ,  $\tau_a = 0.1, 0.25$ , and  $0.5$ , and  $h = 1$  and  $2$  km with the radiometer located at the center of the island: (a)  $\phi = 10^\circ$ ; (b)  $\phi = 90^\circ$ ; (c)  $\phi = 180^\circ$ .

Figure 5. Comparison between the computed values of  $L_t$  as a function of  $R$  with the radiometer at the center and the edge of the island for C80,  $\theta_v = \theta_0 = 60^\circ$ ,  $\tau_a = 0.1, 0.25$ , and  $0.5$ , and  $h = 1$  km: (a)  $\phi = 10^\circ$ ; (b)  $\phi = 90^\circ$ ; (c)  $\phi = 180^\circ$ .

Figure 6. Comparison between the computed values of  $L_t$  as a function of  $R$  with the island's albedo  $A = 0.5$  and  $1.0$ , the radiometer at the center of the island, phase function C80,  $\theta_v = \theta_0 = 60^\circ$ ,  $\tau_a = 0.1, 0.25$ , and  $0.5$ , and  $h = 1$  km.

Figure 7. Comparison between the computed values of  $L_t$  as a function of  $R$  for phase functions C80 and T80, with the radiometer at the center of the island,  $\theta_v = \theta_0 = 60^\circ$ ,  $\tau_a = 0.1, 0.25$ , and  $0.5$ , and  $h = 1$  km.

Figure 8. Relative error in  $L_t$  in the almucantar of the sun ( $\theta_0 = 60^\circ$ ) as a function of the azimuth angle for a radiometer located at the center and edge of the island. For these curves,  $\tau_r = 0.25$ ,  $\tau_a = 0.25$ ,  $h = 1$  km, and  $R = 5$  km.

Figure 9. Comparison between the retrieved and the true values of  $\omega_0 P(\Theta)$  employing simulated sky radiance pseudodata in the absence of the island.  $\tau_r = 0.25$ ,  $\tau_a = 0.25$ ,  $h = 1$  km, and  $R = 5$  km.

Figure 10. Comparison between the retrieved and the true values of  $\omega_0 P(\Theta)$  employing simulated sky radiance pseudodata obtained at the center and the edge of the island.  $\tau_r = 0.25$ ,  $\tau_a = 0.25$ ,  $h = 1$  km, and  $R = 5$  km.

Figure 11. Histogram of the number of occurrences of given values of  $L_t$  in intervals of  $0.0005 \times 10^{-2}$  for 1000 simulations of  $10^4$  photons each, utilizing the method described in the Appendix for computing the contribution  $L_3$ . The dotted line represents the estimate of the mean value of  $L_t$  for the  $10^7$  photons.

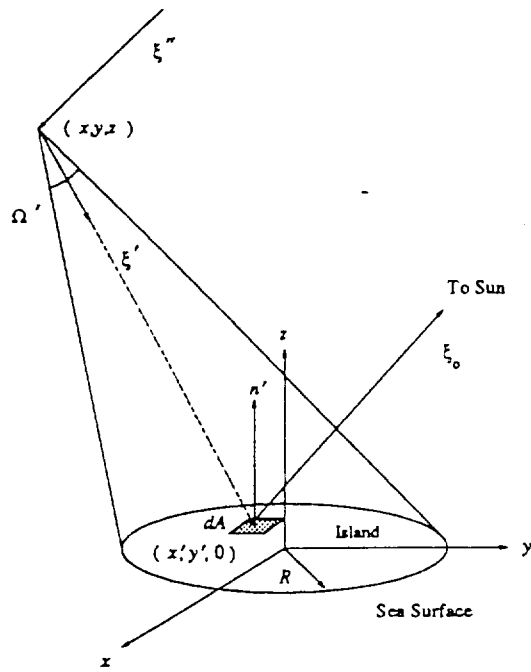


Figure 1. Schematic for computing the island's contribution to the sky radiance.

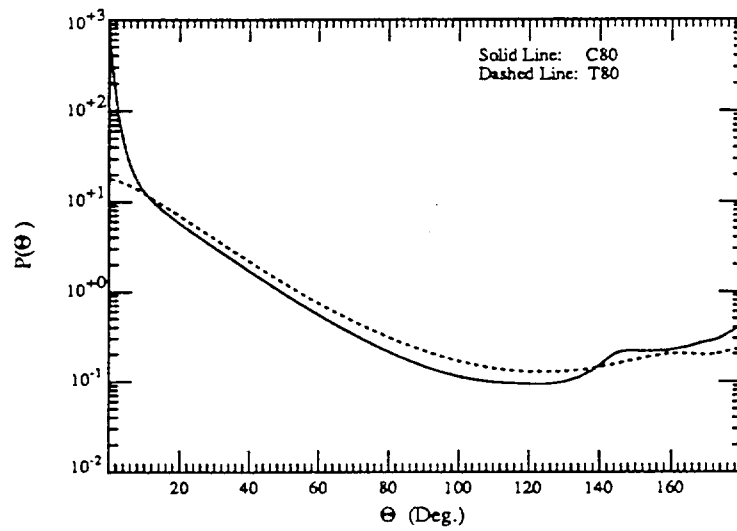


Figure 2. Aerosol scattering phase functions used in the simulations.

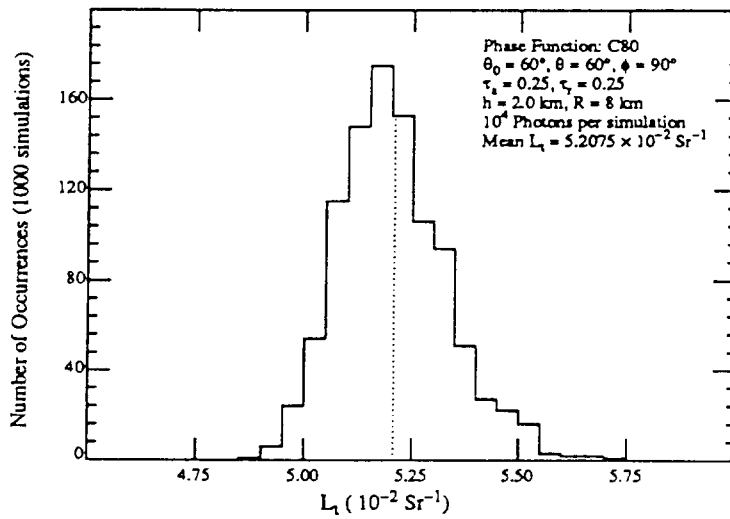


Figure 3. Histogram of the number of occurrences of given values of  $L_t$  in intervals of  $0.0005 \times 10^{-2}$  for 1000 simulations of  $10^4$  photons each. The dotted line represents the estimate of the mean value of  $L_t$  for the  $10^7$  photons.

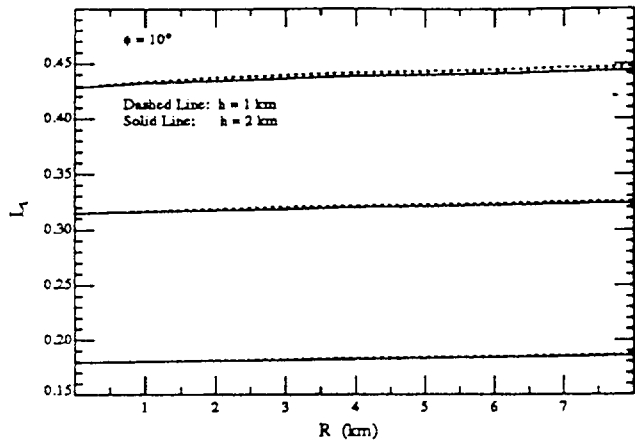


Figure 4a.

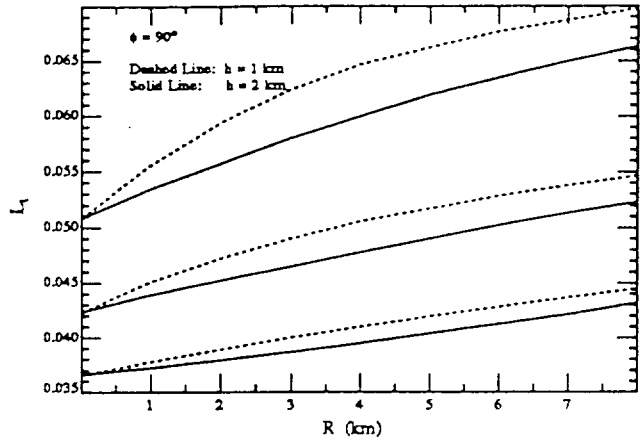


Figure 4b.

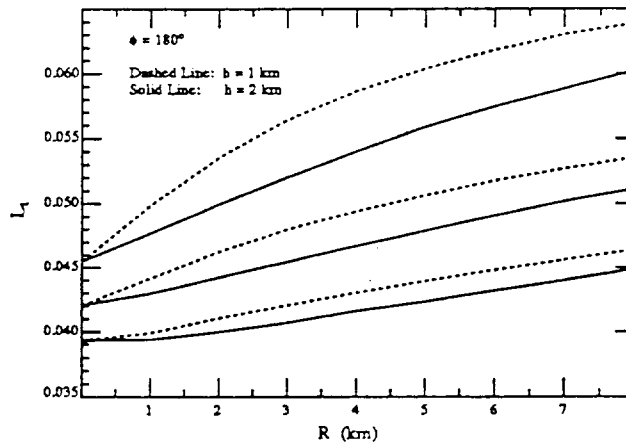


Figure 4c.

Figure 4. Computed value of  $L_t$  as a function of  $R$  for C80,  $\theta_v = \theta_0 = 60^\circ$ ,  $\tau_a = 0.1, 0.25$ , and  $0.5$ , and  $h = 1$  and  $2$  km with the radiometer located at the center of the island: (a)  $\phi = 10^\circ$ ; (b)  $\phi = 90^\circ$ ; (c)  $\phi = 180^\circ$ .

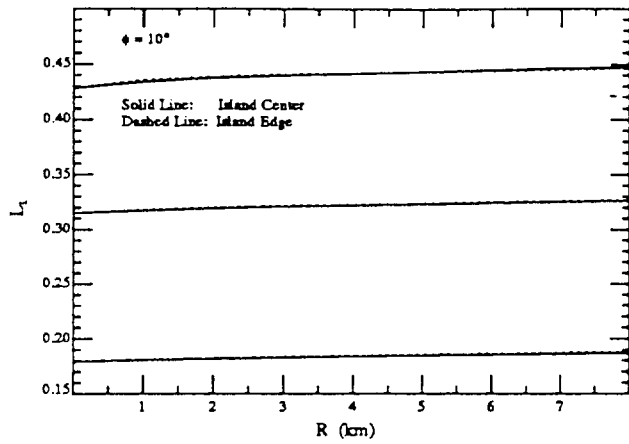


Figure 5a.

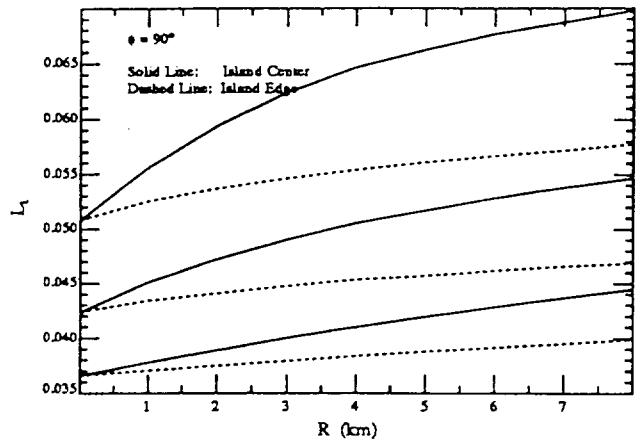


Figure 5b.

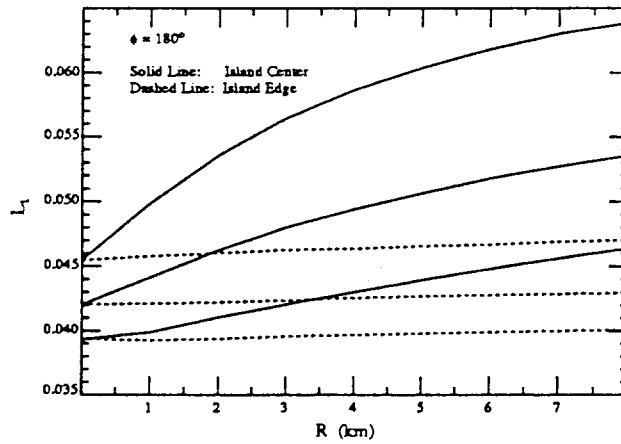


Figure 5c.

Figure 5. Comparison between the computed values of  $L_t$  as a function of  $R$  with the radiometer at the center and the edge of the island for C80,  $\theta_v = \theta_0 = 60^\circ$ ,  $\tau_a = 0.1, 0.25, \text{ and } 0.5$ , and  $h = 1$  km: (a)  $\phi = 10^\circ$ ; (b)  $\phi = 90^\circ$ ; (c)  $\phi = 180^\circ$ .

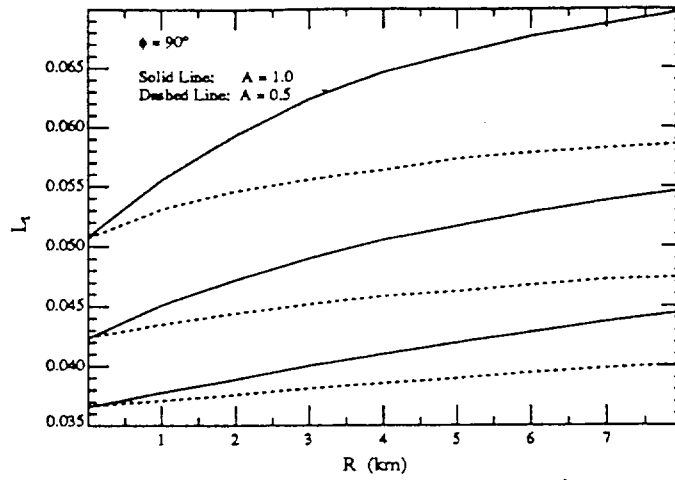


Figure 6. Comparison between the computed values of  $L_t$  as a function of  $R$  with the island's albedo  $A = 0.5$  and  $1.0$ , the radiometer at the center of the island, phase function C80,  $\theta_v = \theta_0 = 60^\circ$ ,  $\tau_a = 0.1, 0.25$ , and  $0.5$ , and  $h = 1$  km.

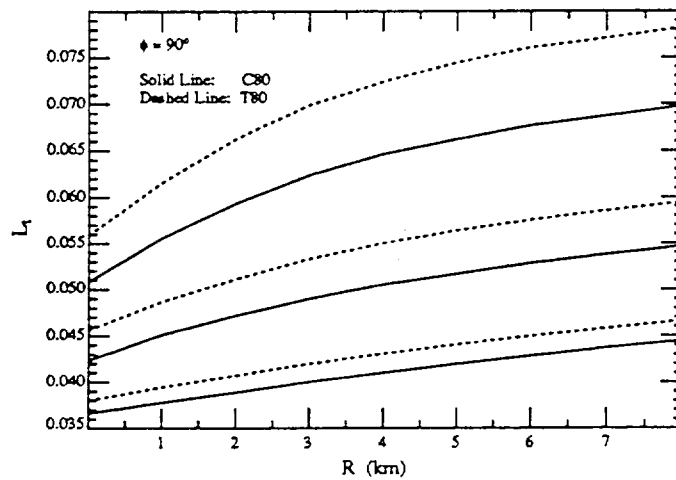


Figure 7. Comparison between the computed values of  $L_t$  as a function of  $R$  for phase functions C80 and T80, with the radiometer at the center of the island,  $\theta_v = \theta_0 = 60^\circ$ ,  $\tau_a = 0.1, 0.25$ , and  $0.5$ , and  $h = 1$  km.

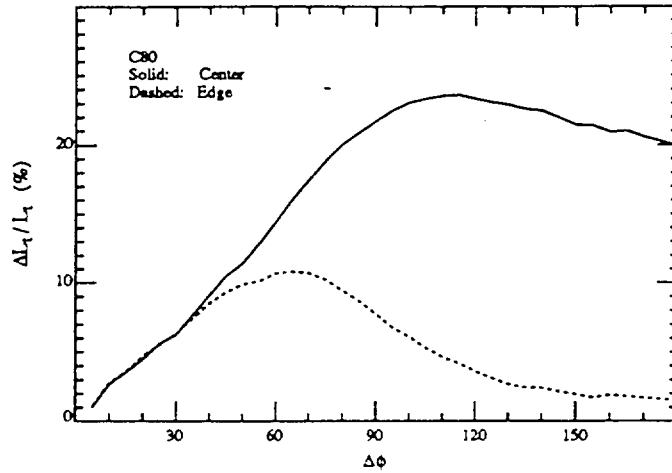


Figure 8. Relative error in  $L_t$  in the almucantar of the sun ( $\theta_0 = 60^\circ$ ) as a function of the azimuth angle for a radiometer located at the center and edge of the island. For these curves,  $\tau_r = 0.25$ ,  $\tau_a = 0.25$ ,  $h = 1$  km, and  $R = 5$  km.

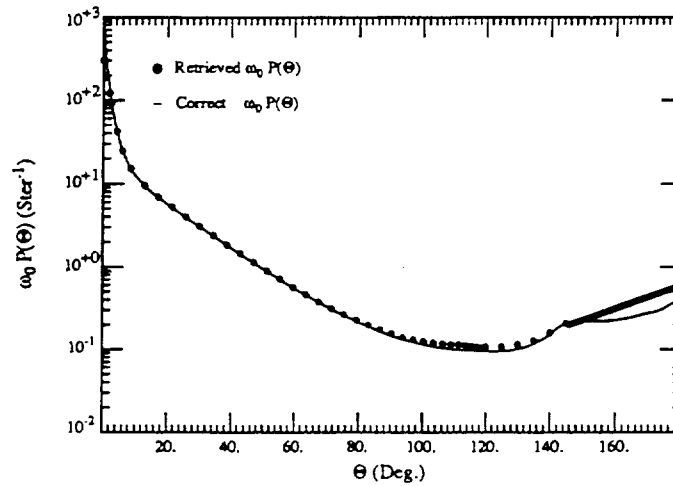


Figure 9. Comparison between the retrieved and the true values of  $\omega_0 P(\Theta)$  employing simulated sky radiance pseudodata in the absence of the island.  $\tau_r = 0.25$ ,  $\tau_a = 0.25$ ,  $h = 1$  km, and  $R = 5$  km.

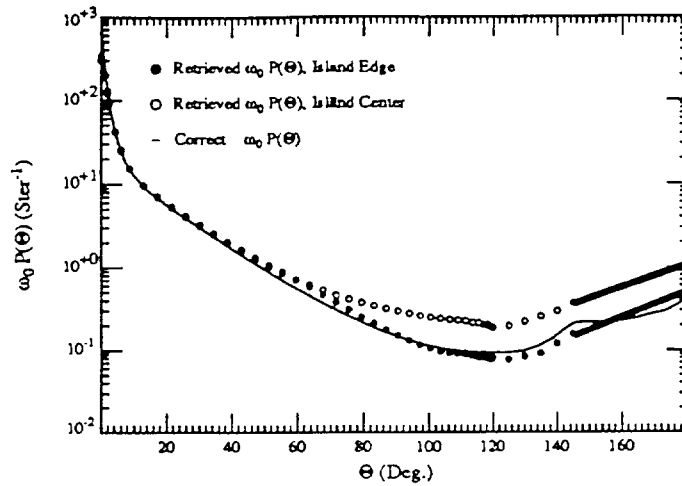


Figure 10. Comparison between the retrieved and the true values of  $\omega_0 P(\Theta)$  employing simulated sky radiance pseudodata obtained at the center and the edge of the island.  $\tau_r = 0.25$ ,  $\tau_a = 0.25$ ,  $h = 1$  km, and  $R = 5$  km.

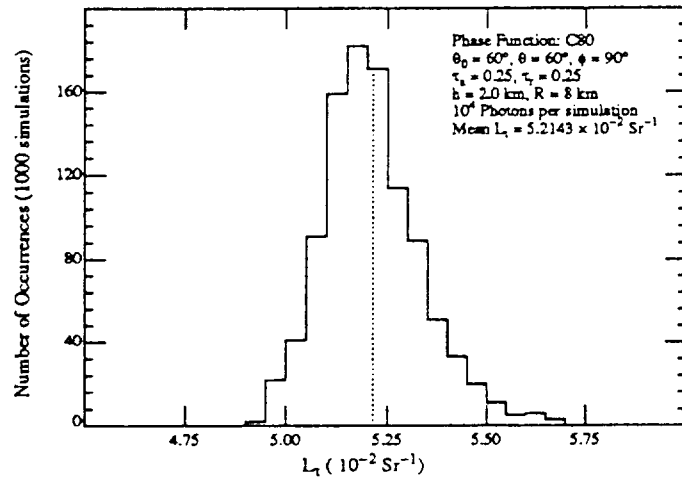


Figure 11. Histogram of the number of occurrences of given values of  $L_t$  in intervals of  $0.0005 \times 10^{-2}$  for 1000 simulations of  $10^4$  photons each, utilizing the method described in the Appendix for computing the contribution  $L_3$ . The dotted line represents the estimate of the mean value of  $L_t$  for the  $10^7$  photons.